SUPPLEMENTARY INFORMATION

The homodimerization domain of the Stl repressor is crucial for efficient inhibition of mycobacterial dUTPase

Zoé S. Tóth[1,2,3,*], Ibolya Leveles[1,2], Kinga Nyíri[1,2], Gergely N. Nagy[1,2], Veronika Harmat[4,5], Thapakorn Jaroentomeechai[6], Oliver Ozohanics[7], Rebecca L. Miller[6], Marina Ballesteros Álvarez[2], Beáta G. Vértessy[1,2,*], András Benedek[1,2,*]

[1] Institute of Molecular Life Sciences, HUN-REN Research Centre for Natural Sciences, Budapest, Hungary

[2] Department of Applied Biotechnology and Food Science, Faculty of Chemical Technology and Biotechnology, Budapest University of Technology and Economics, Budapest, Hungary

[3] Doctoral School of Biology, Institute of Biology, ELTE Eötvös Loránd University, Budapest, Hungary

[4] Laboratory of Structural Chemistry and Biology, Institute of Chemistry, ELTE Eötvös Loránd University, Budapest, Hungary

[5] HUN-REN-ELTE Protein Modelling Research Group, Hungarian Research Network, Budapest, Hungary

[6] Copenhagen Center for Glycomics, Department of Cellular & Molecular Medicine, University of Copenhagen, DK-2200, Copenhagen, Denmark

[7] Department of Medical Biochemistry, Semmelweis University, Budapest, Hungary

[*] To whom correspondence should be addressed. Email: toth.zoe@ttk.hu, benedek.andras@ttk.hu, vertessy.beata@ttk.hu

Supplemental note

Recently we have shown, that the experimentally correct setup of BLI studies require that Stl protein is immobilised on the sensor[1].Table 2 in the main text shows the data for this experiment. As a comparison we also performed the BLI experiment in the setup where MtDUT is immobilised. Comparing data in Table 2 and Table S2 clearly indicates that dimerization of Stl^{WT} interferes with the determination of the binding parameters.

Supplemental tables

Table S1. List of primers used for cloning and mutagenesis

Name	Sequence (5'- 3')
Stl^{NT}_FW	CGAAAAAAGCTAAATTAACTATGAAACCCTGGCGAACACC
Stl^{NT}_Rev	CATAGTTAATTTAGCTTTTTTCGGTATCGGTGCTCAGAATCTG
avi-MtDUT_FW	TATGCTCGAGTATGGGCAGCAGCCATCATC
avi-MtDUT_Rev	GCAGGTACCTCACAAACTCGCATGTCCG
Stl-avi-mut-F-fin	GGCTCAGAAAATCGAATGGCACGAATAACTCGAGCGGCCGCAT
Stl-avi-mut-R-fin	TCGAAGATGTCGTTCAGGCCGGACATGTTGGTATCTTTTTCCAGA ATAATTTTTTTCTGATGTTC
GST-Stl-avi-pan4-F	TATTCTCGAGTATGTCCCCTATACTAGGTTATTGG
GST-Stl-avi-pan4-R	GTCCGGTACCTATTCGTGCCATTCGATTTTCTG
Stl^{NT}-avi_F	ATGTCCGGCCTGAACGAC
Stl^{NT}-avi_R	GCTTTTTTCGGTATCGGTGC

Table S2. BLI interaction analysis of sensor bound MtDUT titrated with Stl.

Ligand	**Analyte**	K_D* **(pM)**	k_{on} **($M^{-1}s^{-1}$)(10^5)**	k_{off} **(s^{-1})(10^{-5})**
$MtDUT^{WT}$	Stl^{WT}	215±2	3.94±0.01	8.44±0.08
$MtDUT^{\Delta loop}$	Stl^{WT}	335±3	2.66±0.02	8.90±0.04
$MtDUT^{WT}$	Stl^{NT}	Heterogenous binding		
$MtDUT^{\Delta loop}$	Stl^{NT}	Heterogenous binding		

* χ^2 value was below 0.4 in all cases.

Table S3. Data collection and refinement statistics

Structure	**MtDUT$^{\Delta loop}$**	**MtDUT-Stl^{NT}**
PDB ID	8CGA	8P8O
Data collection		
Space group	$P6_3$	$P2_12_12_1$
Cell dimensions		
a, *b*, *c* (Å)	55.249, 55.249, 83.751	104.669, 123.82, 170.229
α, β, γ (°)	90.00, 90.00, 120.00	90.00, 90.00, 90.00
Resolution (Å)	47.85-1.26 (1.33-1.26) *	46.38-3.40 (3.50-3.40)
R_{meas}	0.04488 (0.4152)	0.156 (6.237)
I / σI	14.18 (2.69)	13.92 (0.48)
Completeness (%)	99.96 (99.97)	97.50 (93.20)
Redundancy	2.0 (2.0)	5.24 (5.21)
CC1/2	0.996 (0.763)	0.999 (0.314)
Refinement		
Resolution (Å)	47.85-1.30 (1.35-1.30)	46.38-3.40 (3.49-3.40)
No. unique reflections	35602 (3581)	30380 (2113)
R_{work} / R_{free}	0.1413 (0.1618) / 0.1707 (0.2127)	0.2439 (0.5497) / 0.2856 (0.5733)
No. atoms	1231	11820
Protein	1074	11820
Ligand/ion	48	0
Water	117	0
B-factors	14.33	145.65
Protein	13.18	145.65
Ligand/ion	13.26	-
Water	25.29	-
R.m.s deviations		
Bond lengths (Å)	0.007	0.002
Bond angles (°)	1.03	0.48

* Values for the highest resolution shell are shown in parentheses

Table S4. MtDUT^{WT}-Stl^{NT} complex polar interactions

MtDUT^{WT}		Stl^{NT}		Binding type
Residue	**Atom type**	**Residue**	**Atom type**	
His21	NE2	Asn102	OD1	Hydrogen bond
	ND1	Tyr106	OH	
Asp24	OD1			
	OD2			
Arg64	NH1	Tyr116	O	
	NH2			
		Ser115	O	
Ser65	OG	Tyr112	O	
Thr69	OG1	Tyr113	O	
Arg70	NH1	Ser114	O	
		Leu152	O	
Thr81	O	Tyr112	OH	
Asp83	N			
Arg87	N	Tyr106	O	
Lys91	N	Tyr113	OH	
	NZ	Asp110	OD1	Salt bridge Hydrogen bond
Arg110	NH1	Asp117	OD1	Hydrogen bond
	NH2	Tyr116	O	
		Asp117	OD1	Salt bridge Hydrogen bond
Glu126	O	Asn56	ND2	Hydrogen bond
	N		OD1	

Supplemental figures

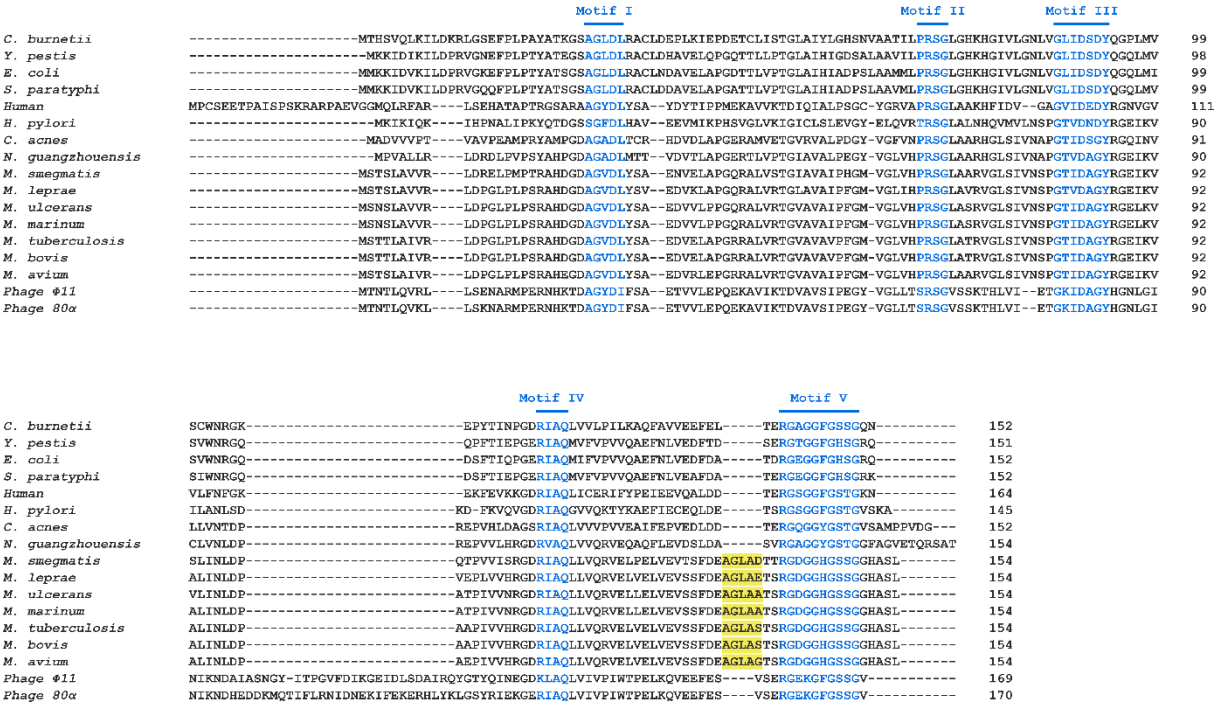

Figure S1. Sequence comparison of several trimeric dUTPase enzymes. The conserved motifs of selected dUTPase sequences are highlighted in blue and indicated as a blue line. The mycobacteria-specific insert sequence elements are highlighted in yellow boxes. The multiple sequence alignment was performed using Clustal Omega.

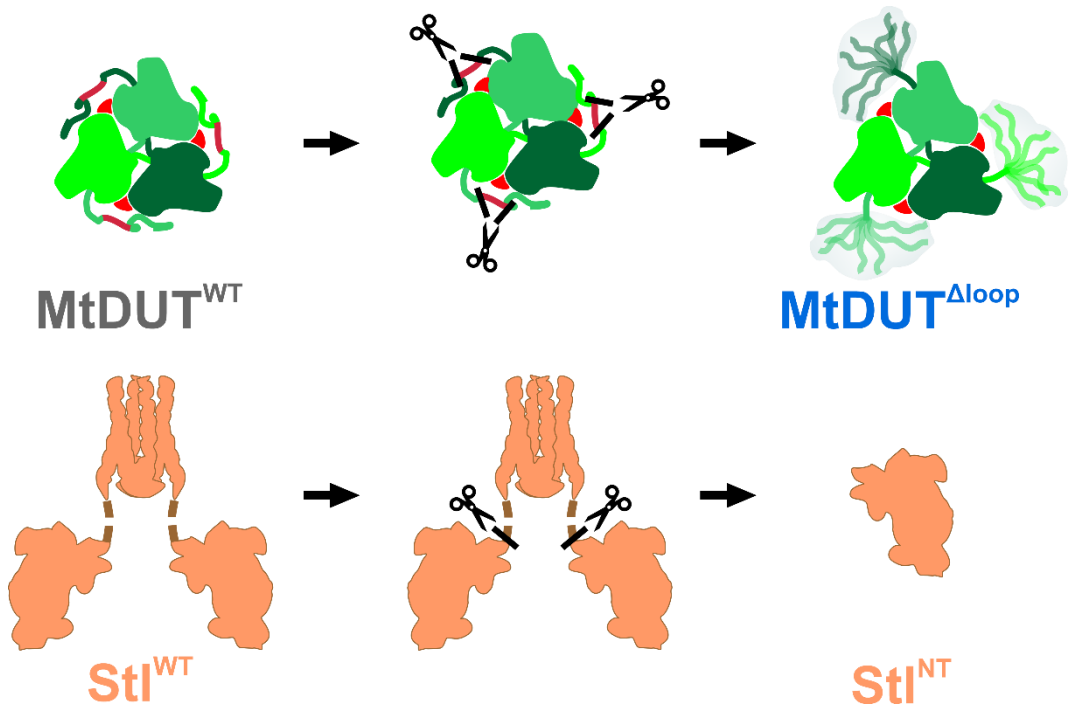

Figure S2. Schematic figure explaining the truncation of MtDUT^{WT} and Stl. The deletion of the AGLAS surface loop of MtDUT^{WT} resulting in MtDUT$^{\Delta loop}$ is shown on the top panel. MtDUT trimers are represented as green figures in three different shades (for the protomers)

(based on crystal structures PDB ID 2PY4 and 8CGA). The C-terminal arm domains are represented as green lines, where the position of the AGLAS surface loop is highlighted in burgundy. For MtDUT$^{\Delta loop}$ the C-terminal arm domains are represented as partially transparent lines. The substrate is shown as red shape. The bottom of this panel shows the truncation of the C-terminal domain of Stl^{WT} resulting in Stl^{NT}. The Stl dimer is represented as a peach -colored figure, which consists of the C-terminal domain (based on crystal structure with PDB ID:6H48) (which is responsible for the dimer formation), the N-terminal domain (based on crystal structure with PDB ID:6H49) and a small hinge region[2] (represented as brown-coloured dashed line) . Stl^{NT} is shown as a peach-coloured figure.

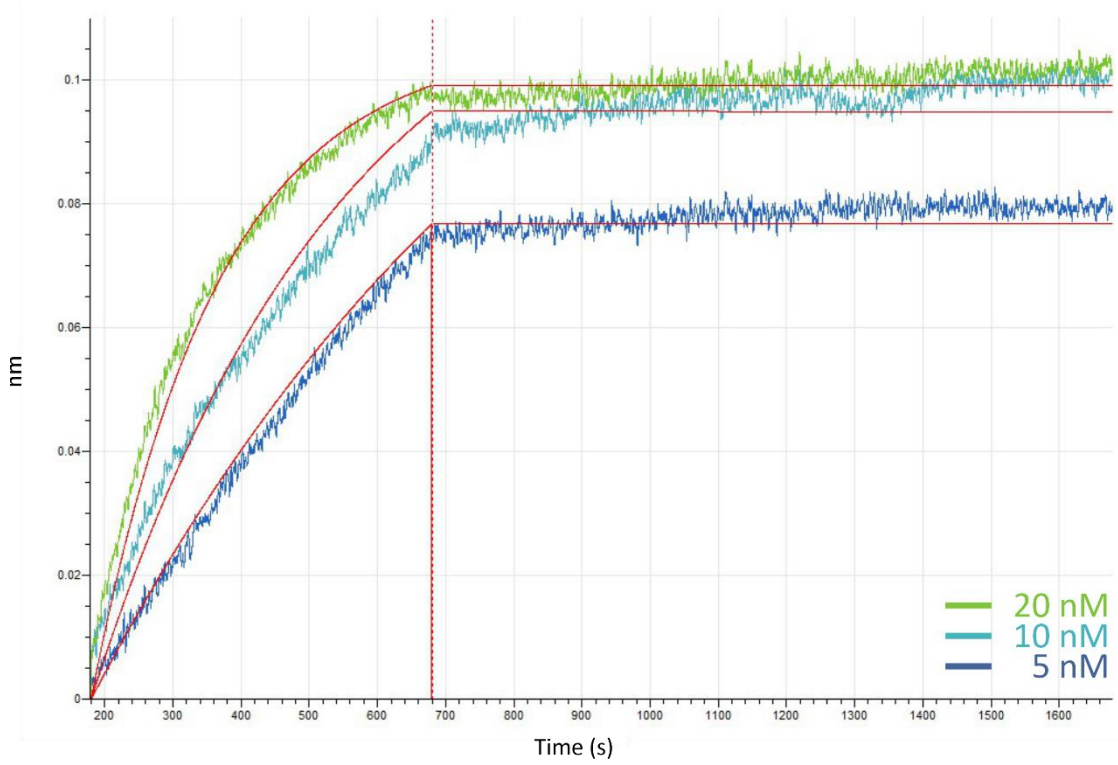

Figure S3. BLI curves of Avi-tagged Stl^{WT} and MtDUT^{WT}. A 1:1 binding model has been fitted to the binding data (K_D<1 pM, χ^2=0.194).

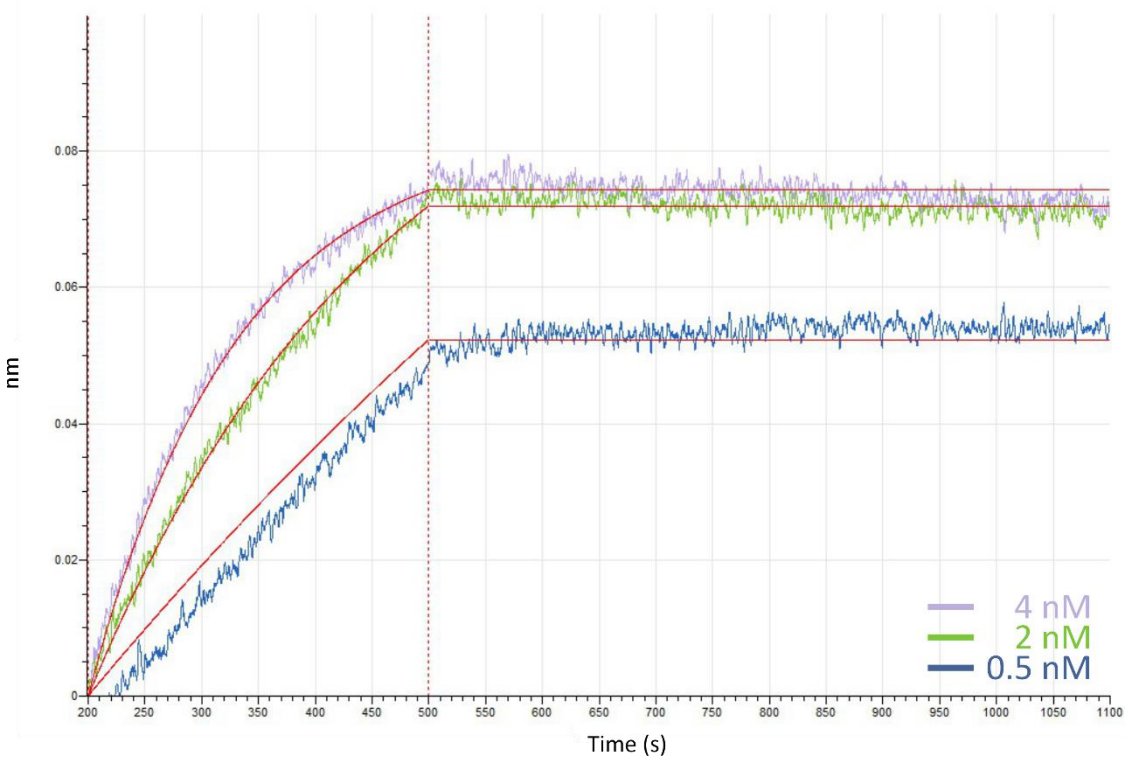

Figure S4. BLI curves of Avi-tagged Stl^{WT} and MtDUT$^{\Delta loop}$. A 1:1 binding model has been fitted to the binding data (K_D=33±1 pM, χ^2=0.0374).

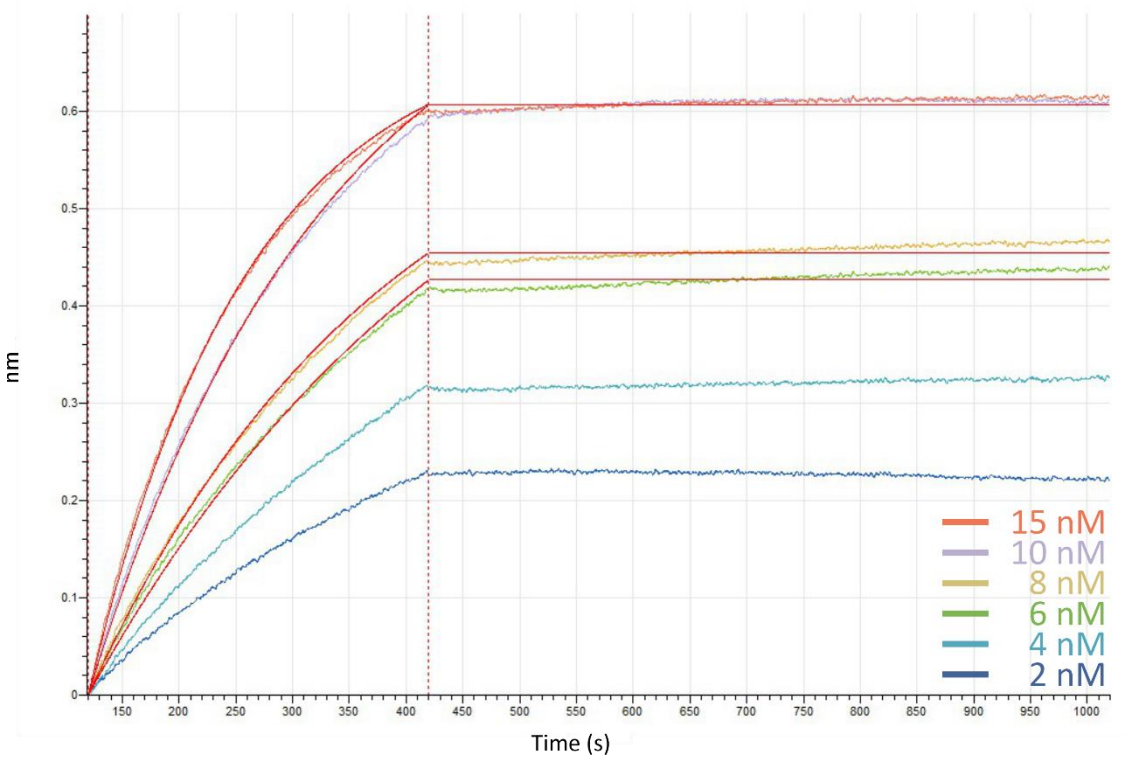

Figure S5. BLI curves of Avi-tagged Stl^{NT} and MtDUT^{WT}. A 1:1 binding model has been fitted to the binding data (K_D=190±1 pM, χ^2=0.2024).

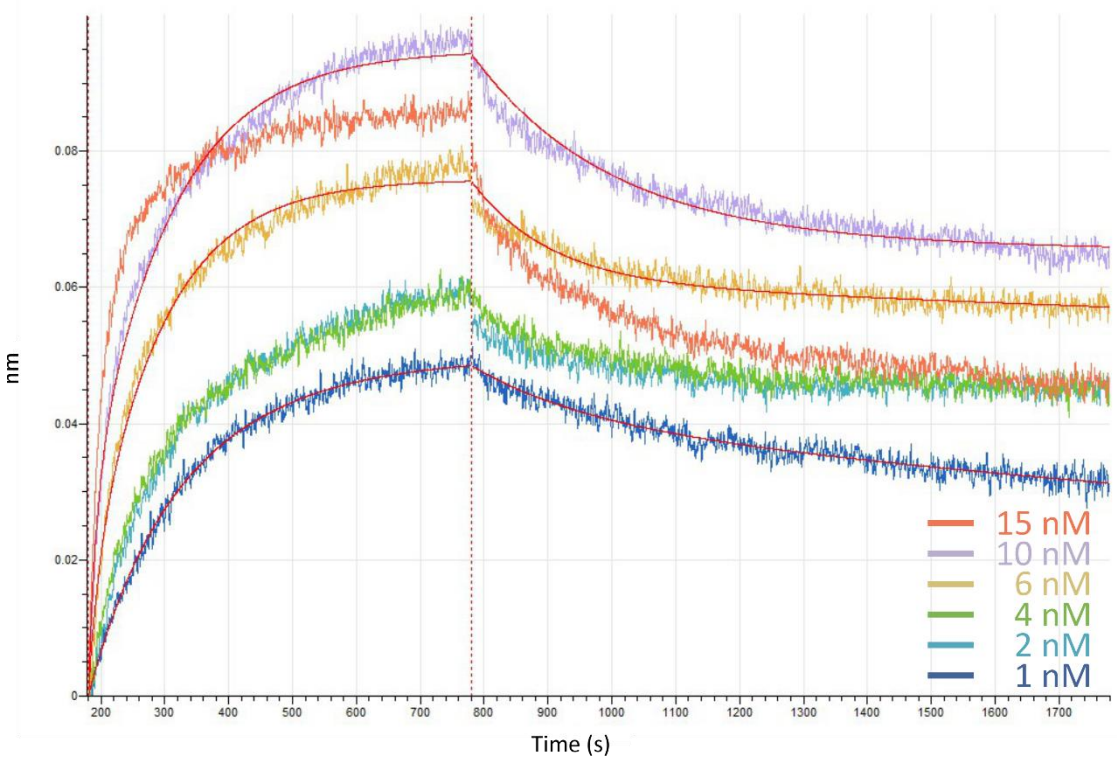

Figure S6. BLI curves of Avi-tagged Stl^{NT} and MtDUT$^{\Delta loop}$. The binding data suggest a case of heterogeneous binding.

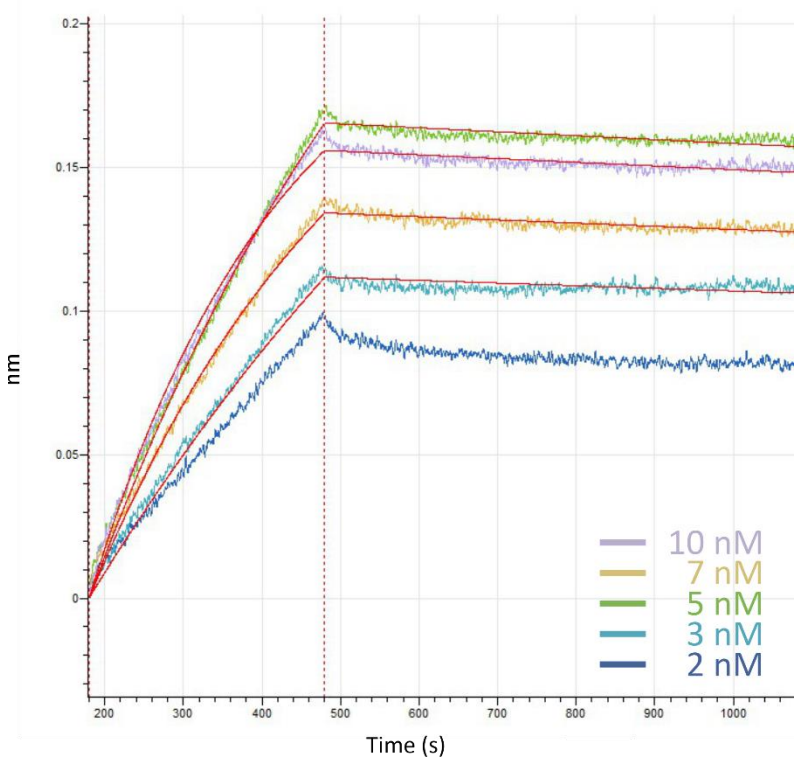

Figure S7. BLI curves of Avi-tagged MtDUT^{WT} and Stl^{WT}. A 1:1 binding model has been fitted to the binding data (K_D=215±2 pM, χ^2=0.0964).

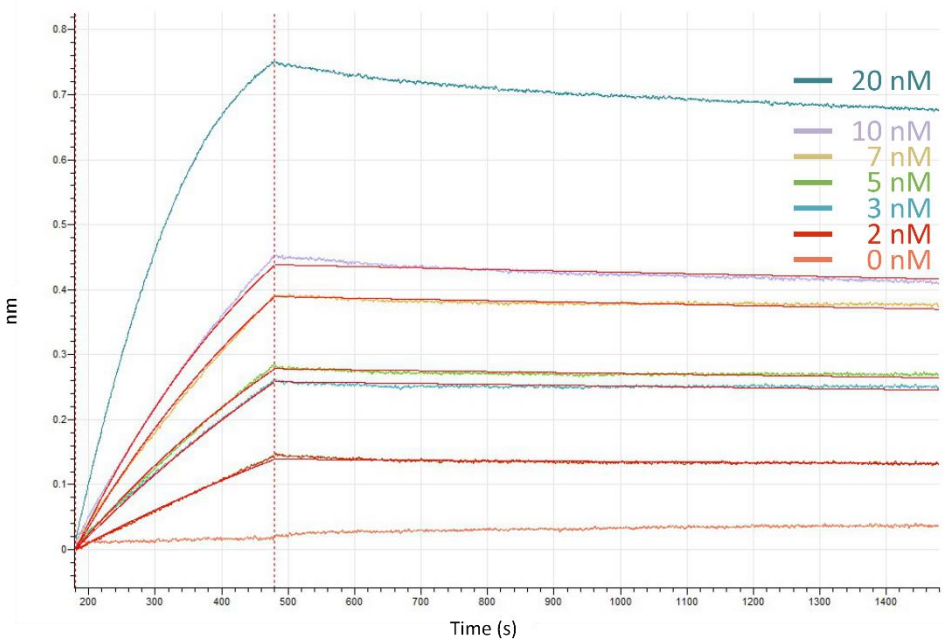

Figure S8. BLI curves of Avi-tagged MtDUT$^{\Delta loop}$ and Stl^{WT}. A 1:1 binding model has been fitted to the binding data (K_D=335±3 pM, χ^2=0.3497).

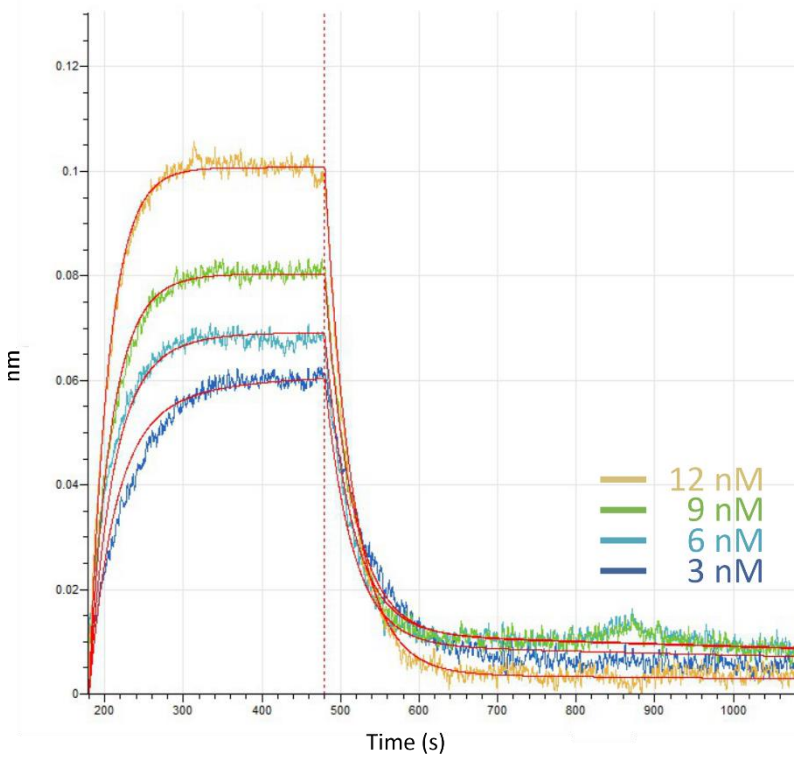

Figure S9. BLI curves of Avi-tagged MtDUT^{WT} and Stl^{NT}. The binding data suggest a case of heterogeneous binding.

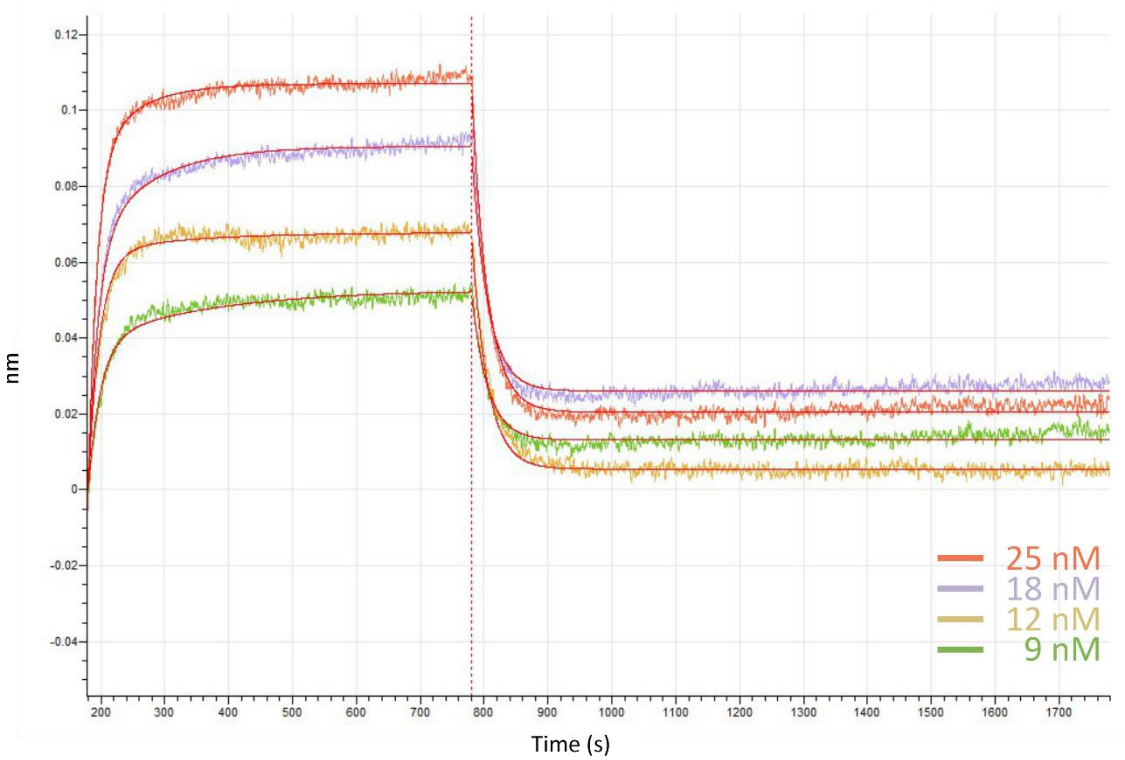

Figure S10. BLI curves of Avi-tagged MtDUT$^{\Delta loop}$ and Stl^{NT}. The binding data suggest a case of heterogeneous binding.

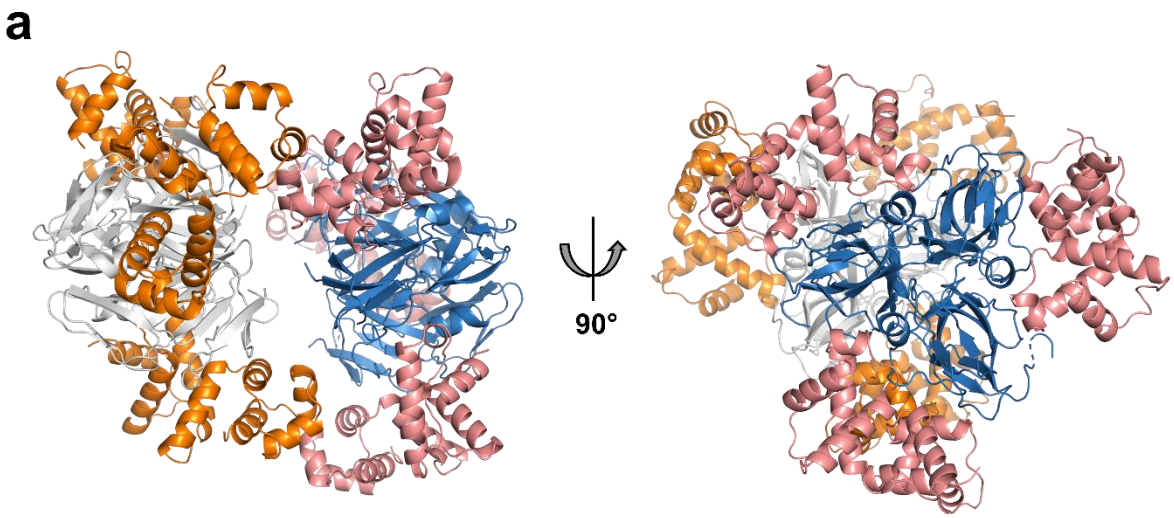
a
90°

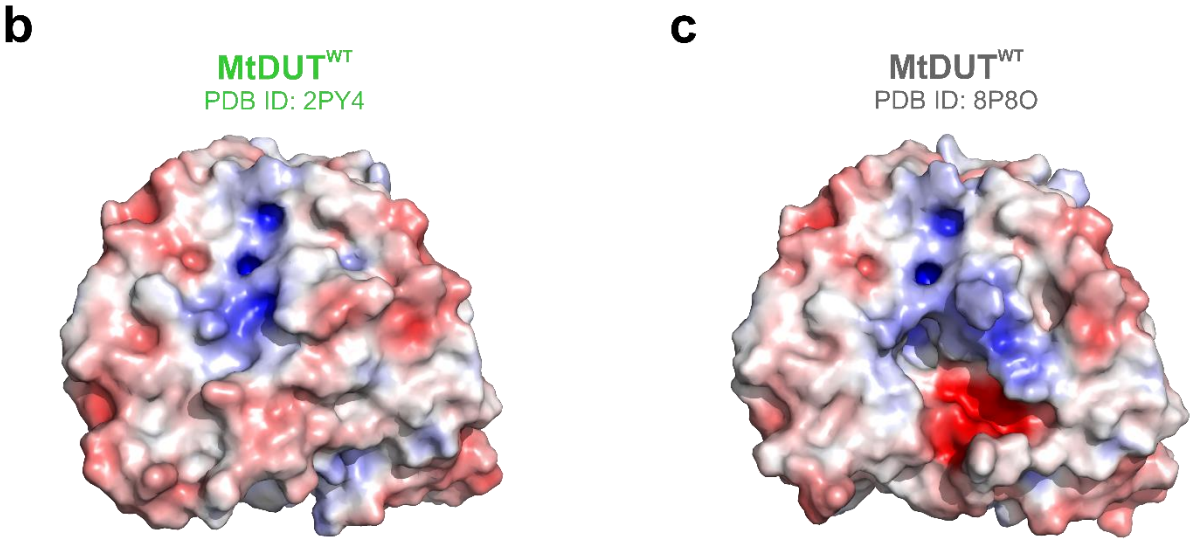
b
MtDUT^WT
PDB ID: 2PY4
c
MtDUT^WT
PDB ID: 8P8O

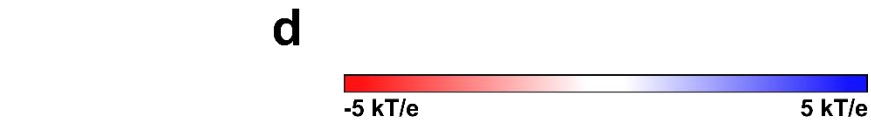
d
-5 kT/e
5 kT/e

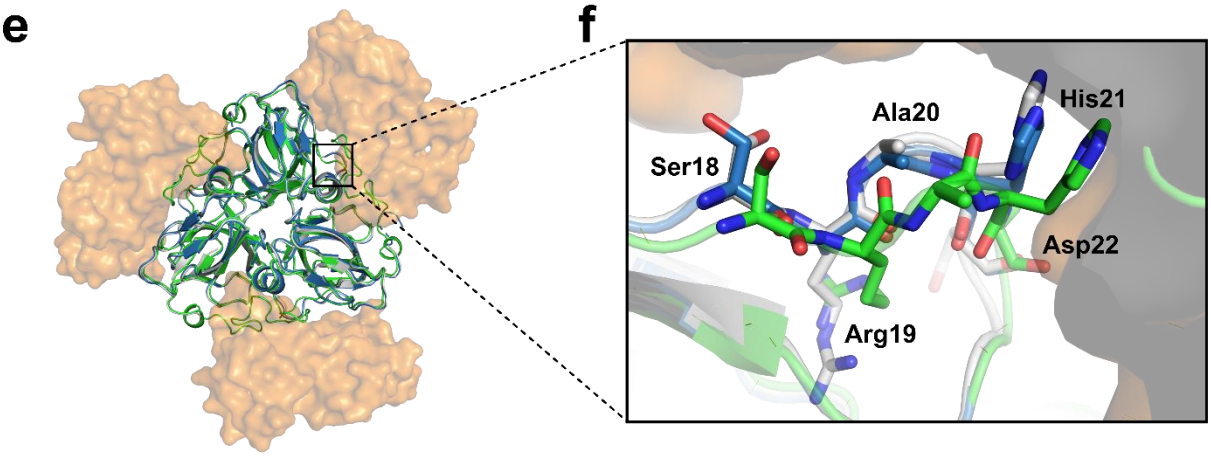
e
f
Ala20
His21
Ser18
Asp22
Arg19

Figure S11. Comparison of MtDUT^{WT} structure in complex with substrate analogue and with Stl^{NT}. a) Composition of MtDUT^{WT}-Stl^{NT} structure asymmetric unit. The two MtDUT^{WT} trimers are displayed as grey and blue cartoons, and StNT monomers are represented as orange and light pink cartoons. b-c) Electrostatic potential of the molecular surfaces of MtDUT^{WT} in complex with dUPNPP substrate analogue (b) (the representation is the same as on Figure 4f) and MtDUT^{WT}in complex with Stl^{NT} (c). d) The colouring of the electrostatic surface potential scale. e) Overall fold comparison of MtDUT^{WT} (PDB ID: 2PY4) and the two MtDUT^{WT} trimers (PDB ID: 8P8O) The two MtDUT^{WT} trimers (PDB ID:8P8O) share a high degree of overall similarity based on root mean square deviation (RMSD) of 0.31 Å for 362 Cα atoms. The deviations from the substrate analogue bound structure based on RMSD values are 0.47 Å and 0.55 Å for 348 and 356 Cα atoms, respectively. MtDUT^{WT} (PDB ID: 2PY4) is represented as green cartoon, MtDUT^{WT} trimers in complex with Stl^{NT} (PDB ID: 8P8O) are represented as grey and blue cartoon and Stl^{NT} is represented as partially transparent orange surface. f) Conformational change of the N-terminal Ser18-Asp22 segment of MtDUT^{WT} upon complex formation with Stl^{NT}. The Ser18-Asp22 peptide segment is highlighted as sticks, the representation of molecules is the same as on panel (e). Individual panels were created using PyMOL 2.5.4 (Schrodinger, LLC; https://www.pymol.org/). The figure was assembled using CorelDRAW 2020 (Corel Corporation; https://www.coreldraw.com).

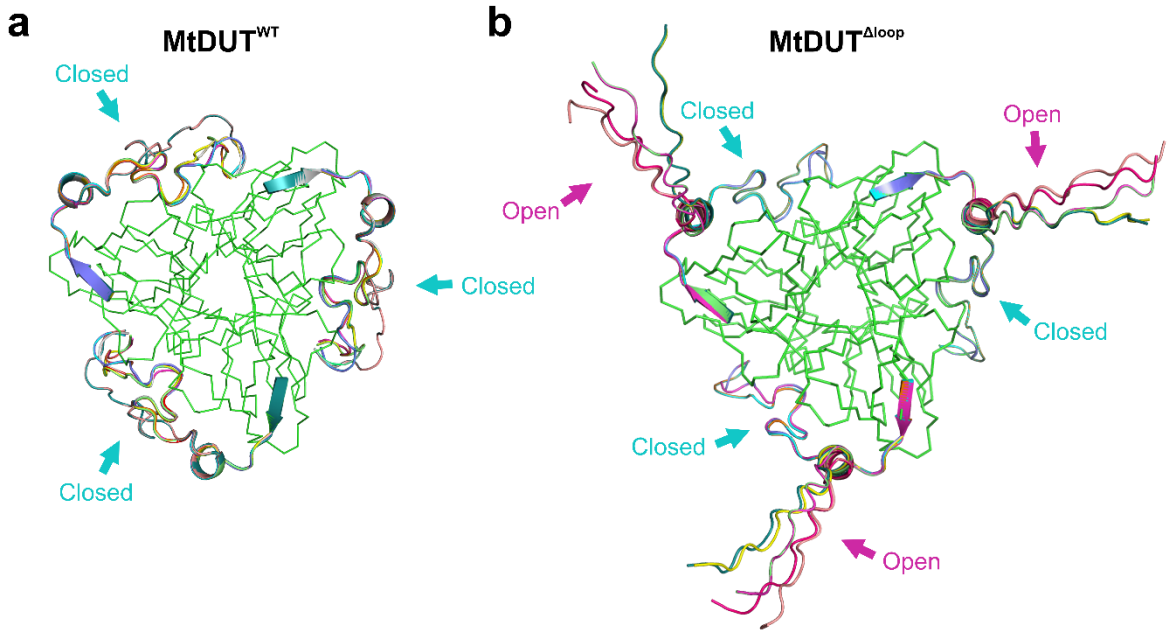

Figure S12. Mobility analysis of C-terminal arm of MtDUT using AlphaFold. a-b) Ten models representing possible conformations of MtDUT^{WT} (a) and MtDUT$^{\Delta loop}$ (b) C-terminal arm. The protein core is shown as green ribbon, the C-terminal domains are shown from the last beta sheet secondary structure element and represented as multiple-coloured cartoons. The turquoise arrows indicate the closed or partially closed conformations of the C-terminal arm, while the magenta arrows indicate the open conformations of the C-terminal arm. The representation of protein structures was created using PyMOL 2.5.4 (Schrodinger, LLC; https://www.pymol.org/). The figure was assembled using CorelDRAW 2020 (Corel Corporation; https://www.coreldraw.com).

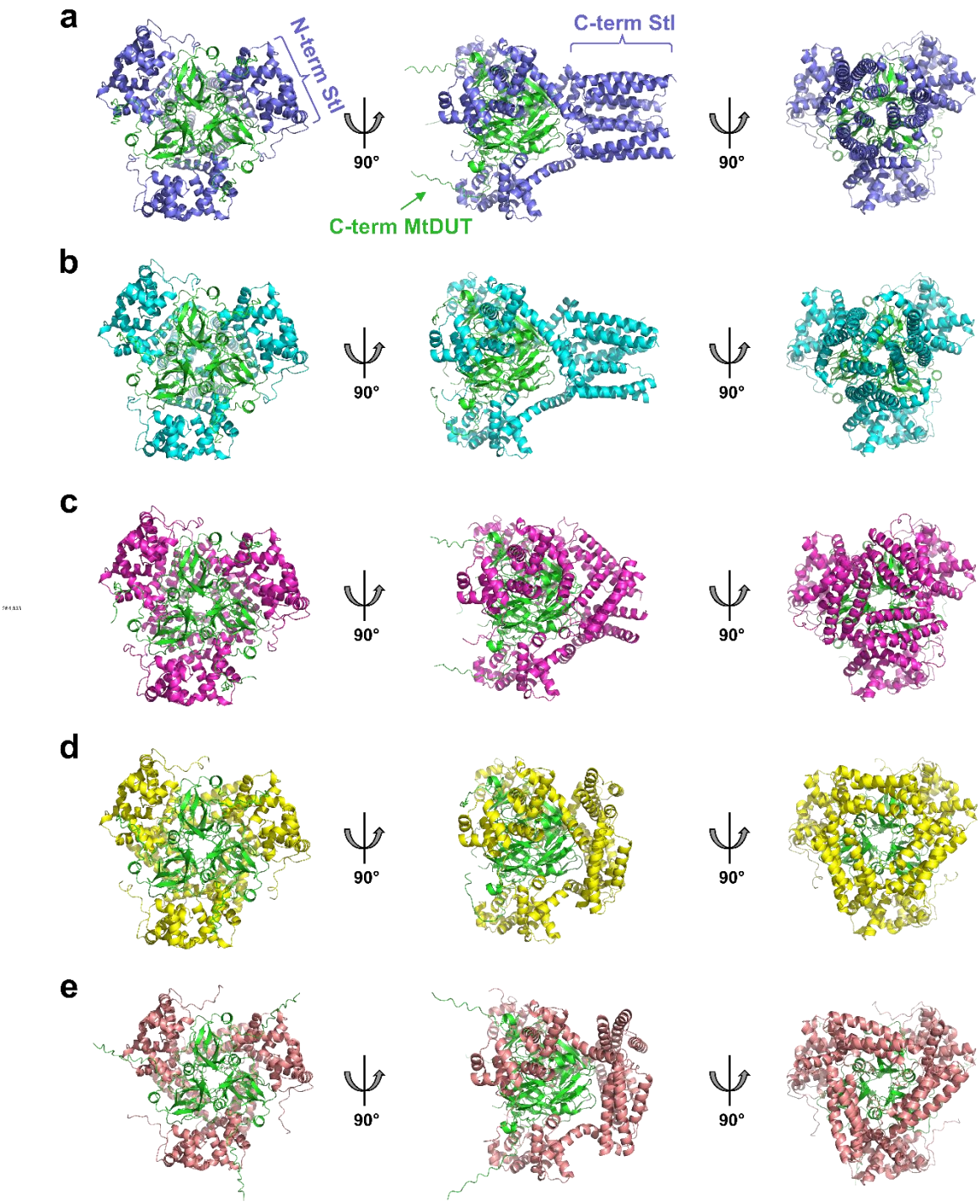

Figure S13. AlphaFold modelling of MtDUT^{WT}-Stl^{WT} complex structure.
a-e) 5 MtDUT^{WT}-Stl^{WT} complex models showing possible complex assemblies of 3:3 binding stoichiometry. The models are shown in 3 different orientations, the MtDUT^{WT} is displayed in green cartoon in all cases, while Stl is represented as different coloured cartoons. Predicted models are in descending order from (a) to (e) based on the prediction ranking scores. The representation of protein structures was created using PyMOL 2.5.4 (Schrodinger, LLC; https://www.pymol.org/). The figure was assembled using CorelDRAW 2020 (Corel Corporation; https://www.coreldraw.com).

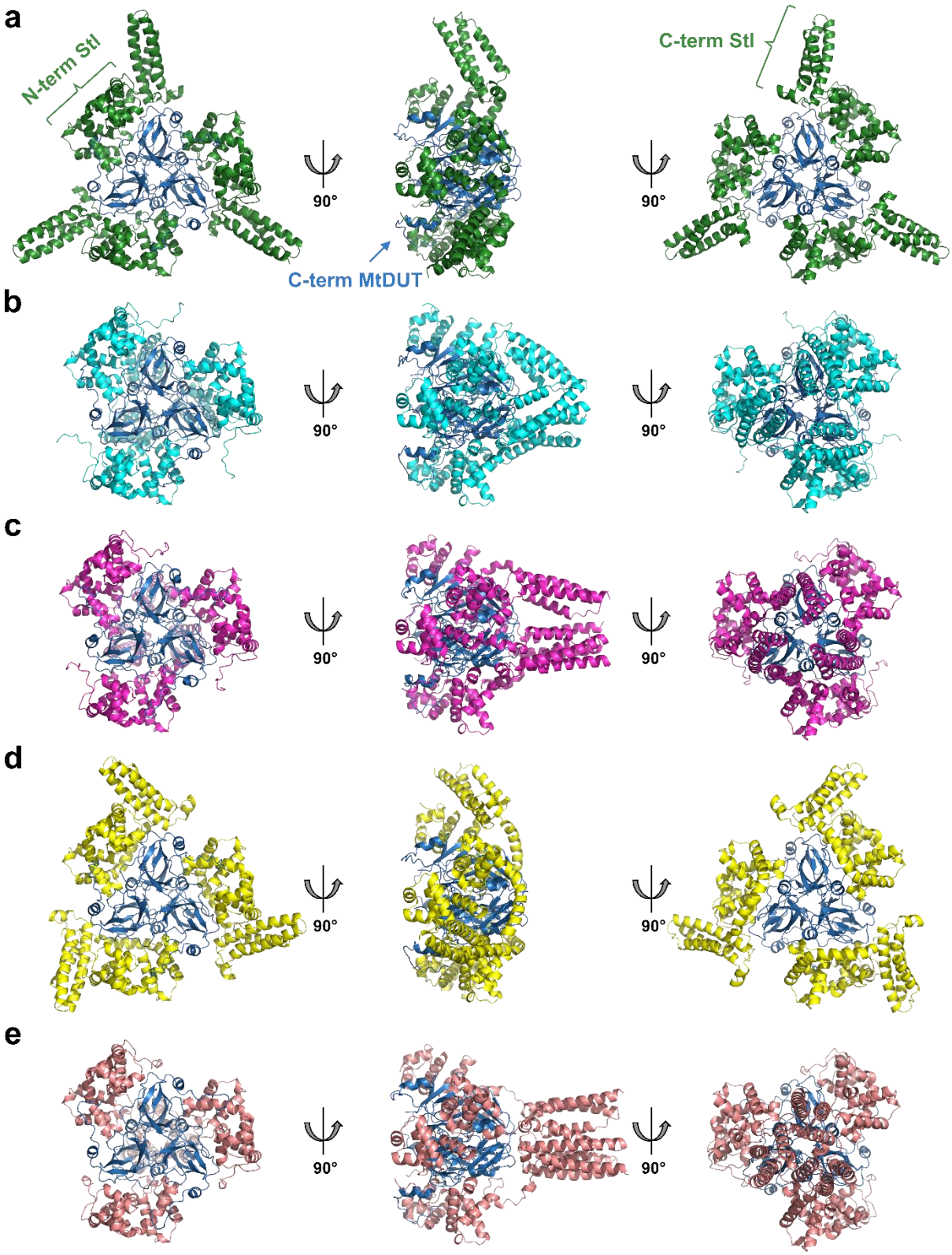

Figure S14. AlphaFold modelling of MtDUT$^{\Delta loop}$-Stl^{WT} complex structure.
a-e) 5 MtDUT$^{\Delta loop}$-Stl^{WT} complex models showing possible complex assemblies of 3:3 binding stoichiometry. The models are shown in 3 different orientations, the MtDUT$^{\Delta loop}$ is displayed in dark blue cartoon in all cases, while Stl is represented as different coloured cartoons. Predicted models are in descending order from (a) to (e) based on the prediction ranking scores. The representation of protein structures was created using PyMOL 2.5.4 (Schrodinger, LLC;

https://www.pymol.org/). The figure was assembled using CorelDRAW 2020 (Corel Corporation; https://www.coreldraw.com).

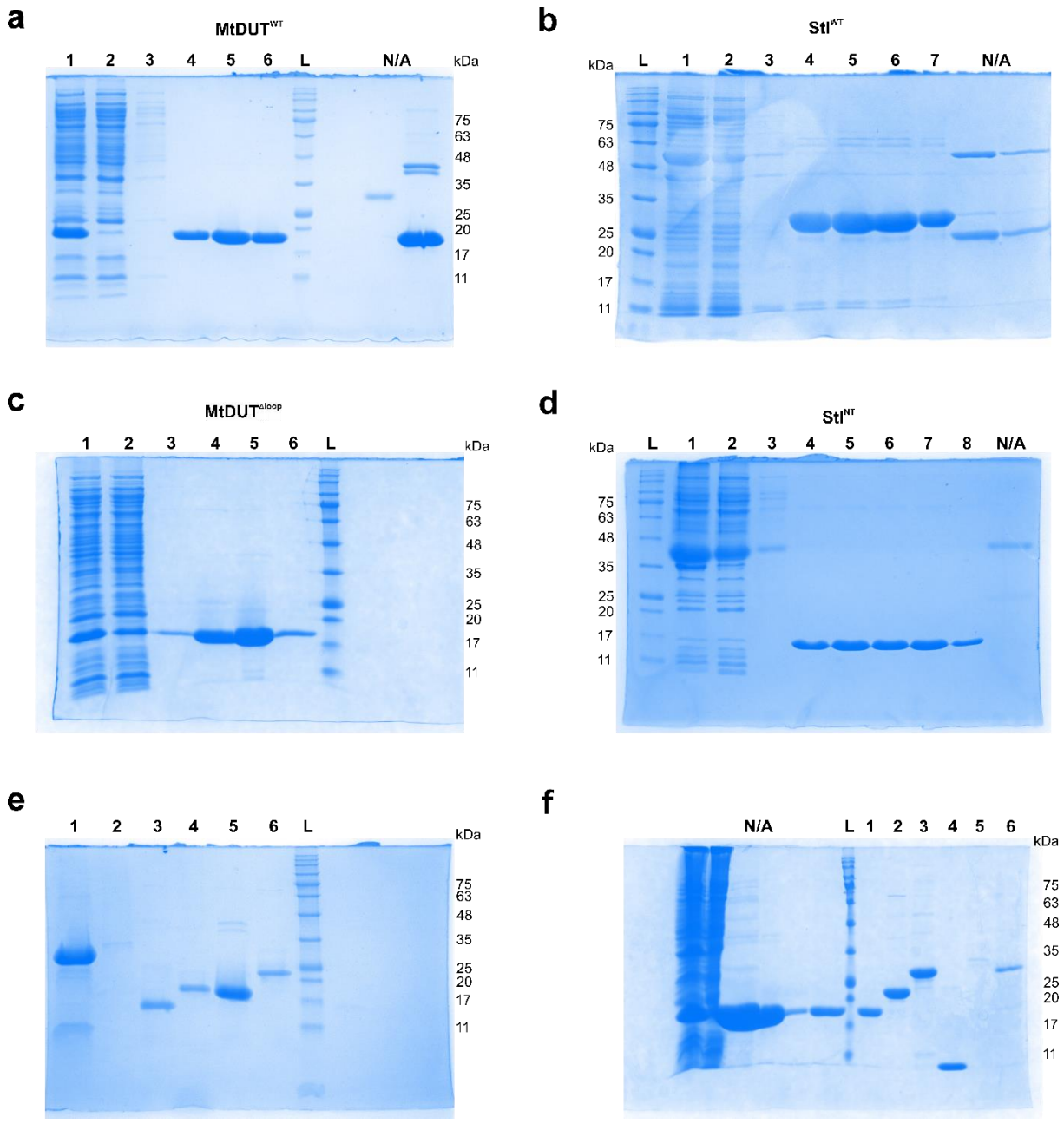

Figure S15. SDS-PAGE images of protein preparations used in this study, purified by affinity chromatography. a) $MtDUT^{WT}$ protein. 1. Supernatant fraction; 2. Flowthrough fraction; 3. Salt wash fraction; 4-6. Elution fractions; L. Protein ladder. b) Stl^{WT} protein. L. Protein ladder; 1. Supernatant fraction; 2. Flowthrough fraction; 3. Salt wash fraction; 4-7. Elution fractions (N/A not applicable). c) $MtDUT^{\Delta loop}$ protein. 1. Supernatant fraction; 2. Flowthrough fraction; 3. Wash fraction; 4-6. Elution fractions; L. Protein ladder. d) Stl^{NT} protein. L. Protein ladder; 1. Supernatant fraction; 2. Flowthrough fraction; 3. Wash fraction; 4-8. Elution fractions (N/A not applicable) e-f) Final protein preparations used in BLI experiments. e) 1. Stl^{WT}; 2. Avi-tagged Stl^{WT}; 3. Stl^{NT}; 4. $MtDUT^{WT}$; 5. $MtDUT^{\Delta loop}$; 6. Avi-tagged $MtDUT^{\Delta loop}$; L. Protein ladder. f) (N/A); L. Protein ladder; 1. $MtDUT^{WT}$; 2. Avi-tagged $MtDUT^{WT}$; 3. Stl^{WT}; 4. N/A; 5. Avi-tagged Stl^{WT}; 6. Avi-tagged Stl^{NT}.

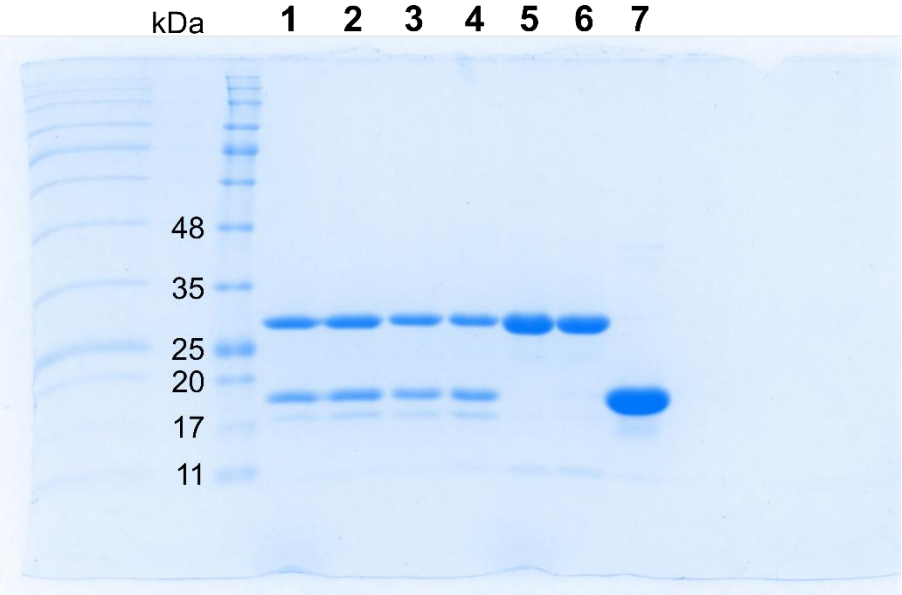

Figure S16. SDS-PAGE image of MtDUT^{WT}, Stl^{WT} proteins and MtDUT^{WT}:Stl^{WT} protein complex analysed by size-exclusion chromatography. 1-3. Protein samples of first peak (peak elution volume: 11.1 ml) of MtDUT^{WT}:Stl^{WT} complex. 4. Protein sample of second peak (peak elution volume: 13.0 ml) of MtDUT^{WT}:Stl^{WT} complex. 5-6. Protein samples of Stl^{WT} peak (peak elution volume: 14.5 ml). 7. Protein sample of MtDUT^{WT} peak (peak elution volume: 14.8 ml).

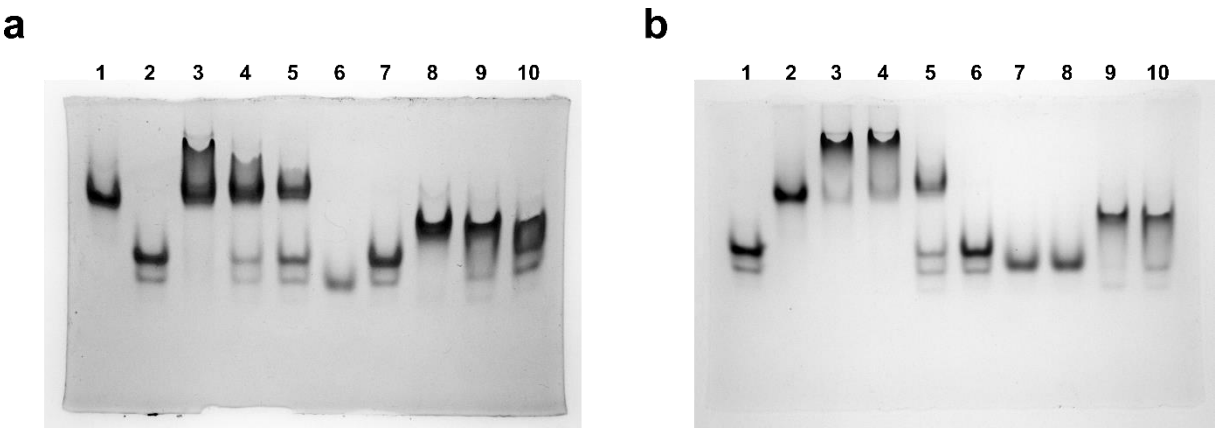

Figure S17. Native gel electrophoresis images analysing MtDUT^{WT}-Stl^{WT} and MtDUT^{WT}-Stl^{NT} complex formation at different mixing concentrations. a) 1. 9 μM Stl^{WT}; 2. 9 μM MtDUT^{WT}; 3. 9 μM Stl^{WT} + 9 μM MtDUT^{WT}; 4. 6 μM Stl^{WT} + 9 μM MtDUT^{WT}; 5. 3 μM Stl^{WT} + 9 μM MtDUT^{WT}; 6. 9 μM Stl^{NT}; 7. 9 μM MtDUT^{WT}; 8. 9 μM Stl^{NT} + 9 μM MtDUT^{WT}; 9. 6 μM Stl^{NT} + 9 μM MtDUT^{WT}; 10. 3 μM Stl^{NT} + 9 μM MtDUT^{WT}. b) 1. 9 μM MtDUT^{WT}; 2. 9 μM Stl^{WT}; 3. 4.5 μM Stl^{WT} + 4.5 μM MtDUT^{WT}; 4. 3.6 μM Stl^{WT} + 5.4 μM MtDUT^{WT}; 5. 2.25 μM Stl^{WT} + 6.75 μM MtDUT^{WT}; 6. 9 μM MtDUT^{WT}; 7. 9 μM Stl^{NT}; 8. 9 μM Stl^{NT}; 9. 4.5 μM Stl^{NT} + 4.5 μM MtDUT^{WT}; 10. 3.6 μM Stl^{NT} + 5.4 μM MtDUT^{WT}.

References

1. Nyíri, K., Gál, E., Laczkovich, M. & Vértessy, B. G. Antirepressor specificity is shaped by highly efficient dimerization of the staphylococcal pathogenicity island regulating repressors: Stl repressor dimerization perturbed by dUTPases. *Sci. Rep.* **14**, 1953 (2024).

2. Ciges-Tomas, J. R. *et al.* The structure of a polygamous repressor reveals how phage-inducible chromosomal islands spread in nature. *Nat. Commun.* **10**, 3676 (2019).